

# Hierarchical Linear-Nonlinear DC Microgrid Control

Juan S. Velez-Ramirez, Eduardo Giraldo

**Abstract**—In this work, a method for hierarchical hybrid linear-nonlinear microgrid control is proposed based on nonlinear primary control and linear secondary control. The nonlinear controller is an Extended Feedback Linearization method, and the linear controller is a PID structure. The proposed method is evaluated in several scenarios to validate its performance to disturbances and island operation mode. To this end, three units of distributed generation are included: Photo-Voltaic Energy Sources, Energy Storage Systems, and Small-Hydro-Power Sources. The results are simulated over a DC microgrid that contains three different distributed generation units with disturbances and island operation mode. As a result, the proposed approach's robustness is validated for several cases, where the advantage of a hierarchical linear-nonlinear structure is shown.

**Index Terms**—Microgrid, hierarchical control, linear, nonlinear.

## I. INTRODUCTION

THE multivariable controller design for microgrids is a task that requires the hierarchical structure that involves controllers with linear and nonlinear features, for example, by using extended feedback linearization controllers for current and voltage [1] to deploy grid feeding or grid forming/supporting nodes respectively, the implementation of multivariable adaptive controllers, when the system is estimated from data [2], or the development of state-space representation based adaptive controllers, where the mathematical modeling is used to describe a linear model of the system dynamics, in order to design a linear controller [3].

Control methods based on hierarchical approaches are presented in [4] where an estimated model of a DC microgrid is controlled due to an LQR regulator in a master-slave configuration. Dynamic energy management algorithm is presented in [5] where the main field is the charging-discharging process of the battery bank. Most of the research on this topic is available in [6].

Control methods that include hierarchical linear-nonlinear strategies are commonly used for microgrid control. For example, in [7], a robust nonlinear control strategy is used to solve the instability problem of DC-DC architectures. Also, in [8] a control method that involves a nonlinear stabilizer is integrated with an extended nonlinear disturbance observer to

achieve closed-loop robustness. Besides, in [9] a Fuzzy logic algorithm is used to connect multiple energy storage systems in a DC-microgrid. Another strategy is presented in [10] by considering a Model Predictive controller with hierarchical structure applied over a Voltage-Source-Converter-Based Microgrid. However, the methods mentioned above are not evaluated under island scenarios to assess their robustness.

In this work, a method for hierarchical microgrid control is proposed based on a primary nonlinear control and a secondary linear cooperative control. The nonlinear controller is an embedded Extended Feedback Linearization method that works in each device as the inner control architecture, whose analysis and results in stand-alone applications are evaluated in [1]. The linear controller is a cascade PID structure that regulates voltage deviation and current sharing in a comparative way, developed in [11]. The results are simulated over a DC microgrid that includes three different distributed generation units: Photo-Voltaic energy sources, energy storage systems, and Small-Hydro-Power sources. The proposed method is evaluated in several scenarios in order to validate its performance by including disturbances and island operation mode. This article is organized as follows: In section II, the primary and secondary control are presented. In section III the results and discussion are shown, and finally, in section IV the conclusions and future works are presented.

## II. THEORETICAL FRAMEWORK

### A. Primary Control: Droop control

The droop control is implemented as a primary control strategy in grid forming and grid supporting converters to neglect the effects of the line's resistance among the DC-link circuit. Equation (1) shows the general form of the droop law, where  $V^{ref}$  is the reference voltage of the converter,  $V$  is the DC-link nominal voltage,  $R_d$  is the droop coefficient, and  $i_o$  is the source current.

$$V^{ref} = V + R_d i_o \quad (1)$$

It is worth noting that the droop law described in (1) has the general form of the line equation. Then, (1) can be graphically represented in Fig 1, in which it is easy to see that the droop gain is the slope of the line.

Manuscript received January 31, 2021; revised May 26, 2021. This work is carried out under the funding of the Universidad Tecnológica de Pereira, Vicerrectoría de Investigación, Innovación y Extensión. Research project: 6-20-7 "Estimación Dinámica de estados en sistemas multivariables acoplados a gran escala".

J.S. Velez-Ramirez is a graduated student at the master on Electrical Engineering program, Universidad Tecnológica de Pereira, Pereira, Colombia. E-mail: jusever@utp.edu.co.

E. Giraldo is a full professor at the Department of Electrical Engineering, Universidad Tecnológica de Pereira, Pereira, Colombia.

Research Group in Automatic Control. E-mail: egiraldos@utp.edu.co.

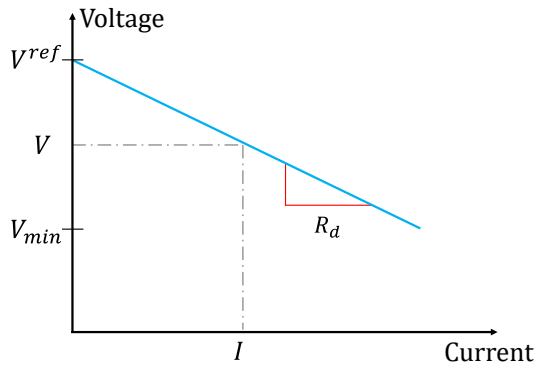


Fig. 1. Voltage vs current graphic based on (1)

For that reason,  $R_d$  must be calculated such that it guarantees the stability of the system. Therefore, the maximum allowable voltage variations and the converter's rated capacity are the factors that must be considered in the droop gain design procedure. This lead expression (2), where,  $I_n$  is the rated current of the converter,  $V_{min}$  is the minimum voltage deviation allowed, and  $V$  is the microgrid nominal voltage.

$$R_d = \frac{V - V_{min}}{I_n} \quad (2)$$

Otherwise,  $R_d$  could be adjusted experimentally with a voltage regulation approach. The droop law (1) can be seen, electrically, as a voltage source ( $V^*$ ) provided by the power electronic device, with ( $R_d$ ) as a virtual series resistance as shown in Fig. 2. This simplified approach eases the simulation process.

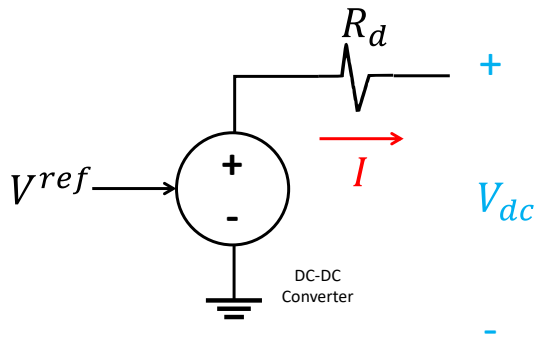


Fig. 2. Simplified droop law circuit approach

Higher droop gains reduce the effect of line resistances on the current sharing accuracy. However, it may cause large voltage drops in the output terminal of the converters [11].

The droop control acts as a primary proportional regulation that establishes the output voltage reference of each converter in a microgrid. Every proportional control has not reference tracking capabilities, resulting in a steady-state error, known as voltage deviation. By itself, the droop law cannot guarantee the proper operation of the microgrid. To correct this issue, a secondary control architecture must be implemented.

### B. Secondary Control

In terms of reliability, efficiency, and sturdiness, it can be said that the centralized architecture is the most accurate option in small microgrid applications [11].

1) *DC link Voltage Regulation*: It is expected that a centralized voltage regulator tracks a reference of the DC-link voltage. In a small microgrid, with a single DC-bus and relatively small line resistance, this task could be accomplished with a simple PI voltage controller as depicted in Fig. 3 (a). Where  $V_{dc}^*$  is the reference voltage of the DC-link,  $V_{dc}$  is the DC-link actual voltage, and  $V^*$  is the voltage reference of the distributed generators.

2) *Current Regulation*: *Proportional power load sharing* is a common term that refers to a percentage sharing of the load, based on the nominal output values of each dispatchable DG unit. Therefore, every DG contributes to the current injection according to its nominal capacity. A PI current control could achieve this goal as depicted in Fig. 3 (b).

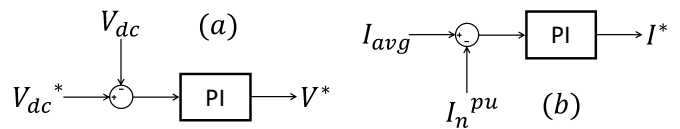


Fig. 3. (a) Voltage regulator, (b) Current regulator

It can be seen from Fig. 3 that  $I_n^{pu}$  is the per-unit value of the current shared by the  $n$  DG, being  $n$  the number of dispatchable units, and  $I_{avg}$  is a value computed by the expression (3)

$$I_{avg} = \text{mean}([I_1^{pu}, \dots, I_n^{pu}]^T) \quad (3)$$

This means that the current regulator has an on-site controller as seen in Fig. 3 (b), and a centralized estimator that computes the current reference (3).

3) *General scheme*: The current regulator output  $I^*$  is added to the voltage regulator output  $V^*$  to compute the reference voltage of the droop law  $V^{ref}$ . The per-unit value of the injected current  $I_n^{pu}$  is computed by using (4), where  $I$  is the actual value of the injected current, and  $I_{nom}$  is the nominal current of the DG unit.

$$I_n^{pu} = \frac{I}{I_{nom}} \quad (4)$$

The hierarchical control scheme until the second layer is summarized in Fig. 4, where  $[R_1, \dots, R_n]$  are the line resistances, and  $[R_{L1}, \dots, R_{Li}]$  are the load resistances being  $i$  the number of loads.

## III. RESULTS AND DISCUSSION

### A. Experimental Setup

In Fig. 5 is shown the general structure of the microgrid tested in the simulation tool. Three different DGs with different line resistances are connected to a common DC-bus [1]. Note the switches  $S_1, S_2$  are included to simulate two different disturbances. All the variables involved in the microgrid control are average values due to the converters' commutation, which causes interruptions in the current flux.

1) *Model Constants*: The inner constant parameters of the converters: inductance, and capacitance, are the same of [1]. In order to test the EFL method in different conditions, some variations are considered in each of the converters and the whole microgrid operation. Table I refers the properties of the grid forming/supporting nodes which inner control strategies is the voltage controller described in [1].

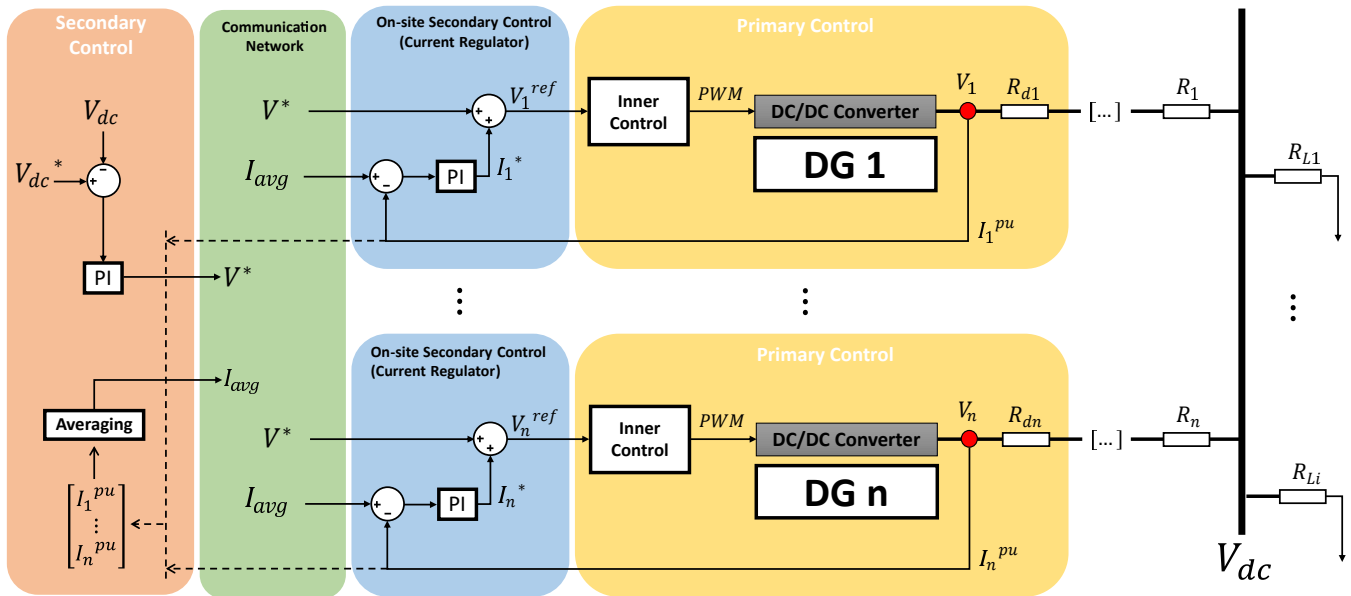


Fig. 4. Diagram of a centralized control architecture with voltage and current regulation

TABLE I  
GRID FORMING/SUPPORTING CONVERTERS NOMINAL PARAMETERS

FORMING/SUPPORTING NOD	NAME	VALUE
Utility Grid (Forming)	Input Voltage (controlled Variable)	-
	Output Voltage (controlled Variable)	380V
	Nominal Inductor Current (controlled variable)	30A
	Line Resistance	0.01Ω
Small Hydro-power (supporting)	Drop Coefficient $R_d$	0.09Ω
	Input Voltage (controlled Variable)	1200V (Nominal)
	Output Voltage (controlled Variable)	380V
	Nominal Inductor Current (controlled variable)	25A
	Line Resistance	0.204Ω
	Drop Coefficient $R_d$	0.1Ω

Table II refers the parameters of the grid supporting nodes that have integrated the current controllers developed in [1]. The nominal inductor current parameter is used as current references in order to simulate the Maximum Power Point Tracker operation.

TABLE II  
GRID FEEDING (CURRENT CONTROL) CONVERTERS NOMINAL PARAMETERS

DG NODE	NAME	VALUE
Photovoltaic	Input Voltage	760V
	Nominal Inductor Current (controlled variable)	20A
	Line Resistance	0.4Ω
Battery Energy Storage	Drop Coefficient $R_d$	0.09Ω
	Input Voltage	645V
	Nominal Inductor Current (controlled variable)	15A
	Line Resistance	0.2Ω

The parameters of the load-side converters are depicted in Table III.  $L_1$  converter isolates a 48V DC-link, and  $L_2$  isolates a 36V DC-link. The purpose of these devices is to imitate a microgrid with different voltage levels. To simplify the simulation, the considered AC loads are changed for  $L_3$ . It is worth noting that this node is directly connected to the DC Voltage line and has a relatively low resistance value.

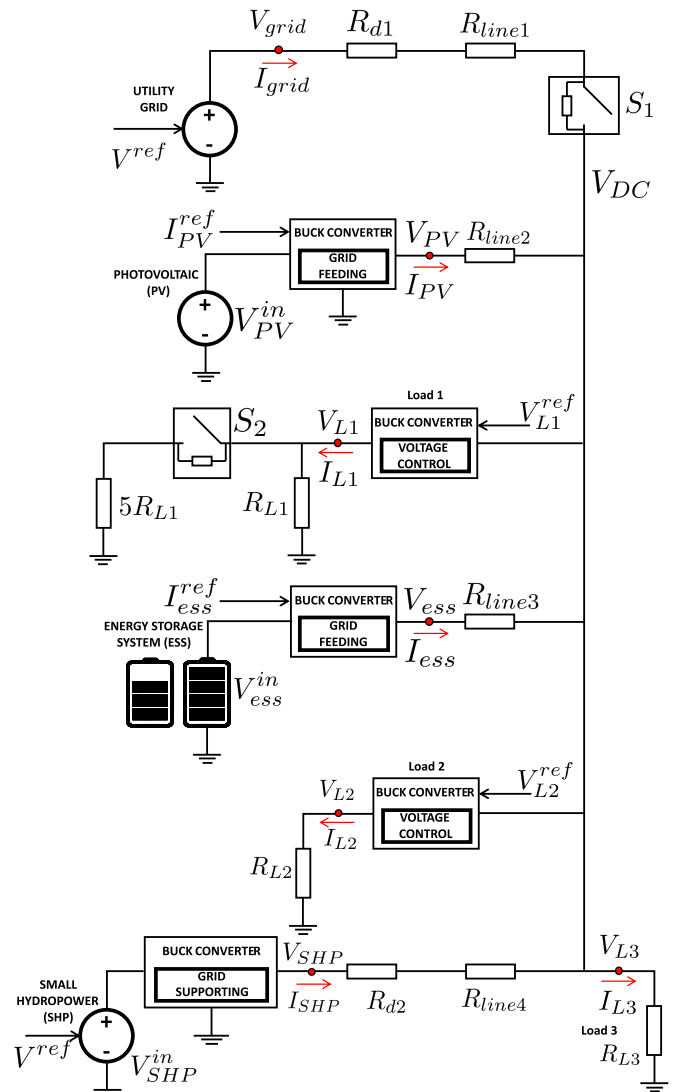


Fig. 5. Experimental setup of the micro-grid

TABLE III  
 DC-DC LOAD INTERFACES NOMINAL PARAMETERS

Load Converters Nominal Parameters	NAME	VALUE
Load 1	Input Voltage	380V
	Output Voltage (controlled variable)	48V
	Nominal Inductor Current	41.66A
	Nominal Resistance ( $R_{L1}$ )	1.1520 $\Omega$
Load 2	Input Voltage	380V
	Output Voltage (controlled variable)	36A
	Nominal Inductor current	31.25A
	Nominal Resistance ( $R_{L2}$ )	1.1520 $\Omega$
Load 3 (Directly Connected to the DC-link)	Input Voltage	380V
	Nominal Resistance ( $R_{L3}$ )	7 $\Omega$

The constants of the EFL have to be adjusted in each new design of the buck converters. The new gains are specified in Table IV. Each case required an experimental adjustment.

 TABLE IV  
 EFL CONTROL CONSTANTS

Converter Node	CONSTANT	VALUE
Photo-voltaic, Energy Storage	K	6060
	$K_i$	-3.6e5
Small Hydro-power	$K_1$	1.36e5
	$K_2$	820
	$K_i$	-2.4e6
Loads 1, 2	$K_1$	12.474e6
	$K_2$	15.83e3
	$K_i$	-36e7

The PI constants of the voltage and current regulator are shown in Table V. The tuning of these gains are made through experimental analysis.

 TABLE V  
 PI CONTROL REGULATORS CONSTANTS

PI CONTROLLER	CONSTANT	VALUE
Current regulator	$K_i$	1600
	$K_p$	800
Current Regulator	$K_i$	200
	$K_p$	0.5

2) *Simulation Settings:* The simulation is developed in Matlab-Simulink® with a duration of 800ms. All control references begin with their nominal values. Grid Forming node's output voltage is controlled by the voltage and current regulator as depicted in Fig. 4 and Fig. 5. Their references are the DC-link nominal voltage (380V) and the estimated average current ( $I_{avg}$ ). In order to test the controllers' robustness, two different disturbances are programmed in the switch's  $S_1$  and  $S_2$ . The first one at  $t = 250ms$ ,  $S_2$  normally open, is closed, inducing a parallel connection of a resistive load equal to  $5R_{L1}$ , simulating a sudden load increase in  $L_1$  node. The second one is the disconnection of the utility grid at 310ms, when normally closed  $S_2$  is opened, simulating a forced isolating of the microgrid, testing the capacity of the SHP node of maintaining the DC-link voltage, and all interfaces sturdiness.

### B. Experimental Results

In Fig. 6 is shown the current behavior for all the DG units, wherein Fig. 6(a) is shown the response through all the simulation. In Fig. 6(b) is shown a zoom of the transient response in which is evident a high overshoot of the grid current of 16.223A around 100% of the steady-state value, is evident that all the DG units have better behavior. The overall settling time is approximately 20ms.

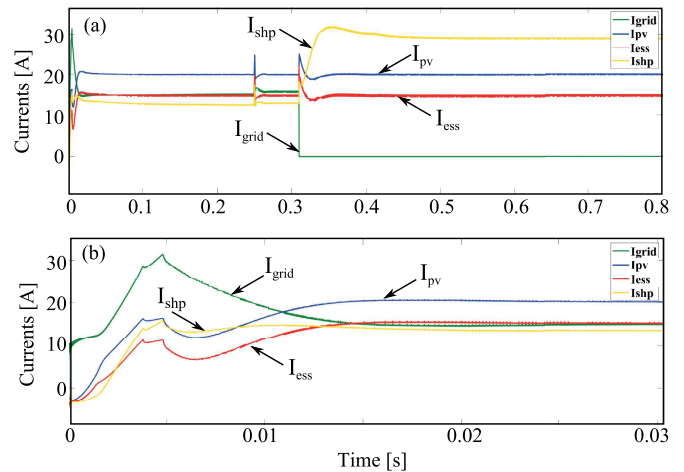


Fig. 6. (a) DGs current injection response. (b) Transient state response.

In Fig. 7(a) is shown a zoom of the response against the first disturbance. It is worth mentioning that a medium overshoot of 6.761A is visible among all the DGs. The settling time is around 15ms, and it is noticeable how the dispatchable units work together to supply the extra load current requirement. In Fig. 7(b) it is shown the zoom of the isolation behaviour, at  $t = 310ms$  the utility grid is disconnected through the opening of  $S_1$ . The new grid forming node is now the SHP generator, and it is easy to see how the current injection of this node grows proportional to the supply loss of the utility grid. The overshoot for SHP is 2.8633A, around 9.87% of the steady-state value and, the grid feeding sources experiment a disturbance of 6A despite the PV node and 7A for  $E_{ss}$  node. The whole isolation process has a settling time of 328ms.

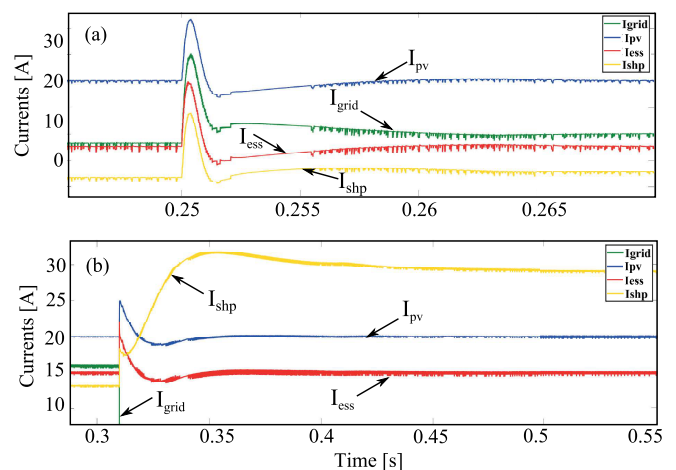


Fig. 7. (a) Load Connection response. (b) Grid Disconnection-Island operation mode

In Fig. 8 is shown the behaviour of the DGs output voltage, where Fig. 8(a) is the whole simulation graphic and Fig. 8(b) is the transient state response zoom, showing a smooth transition with a negligible overshoot of 6.19V around 1.63% of the steady state value and a estimated settling time of 50ms.

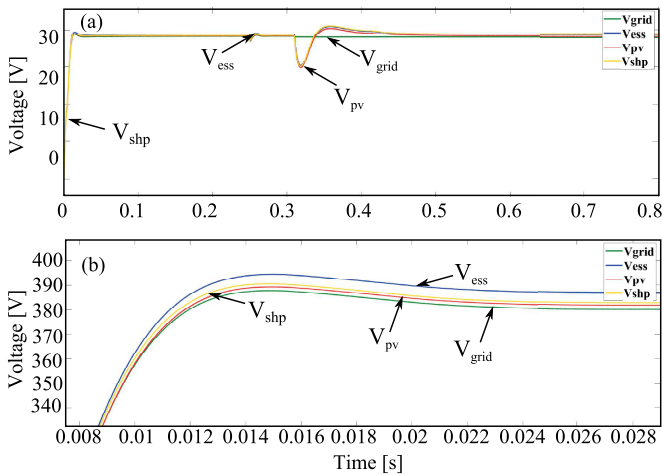


Fig. 8. (a) DGs Voltage output. (b) Transient state response.

In Fig. 9 is shown the behaviour of the DGs output voltage. In Fig. 9(a) it is shown the response against the first disturbance, with an average voltage loss of 13.07V around the 3.5% of the steady-state value and a settling time of 26.9ms. Finally, in Fig. 9(b) a considerable oscillation is triggered by the utility grid disconnection, the voltage loss reaches 85.06V a 23% of the steady-state value, but the disturbances is controlled in approximately 190ms.

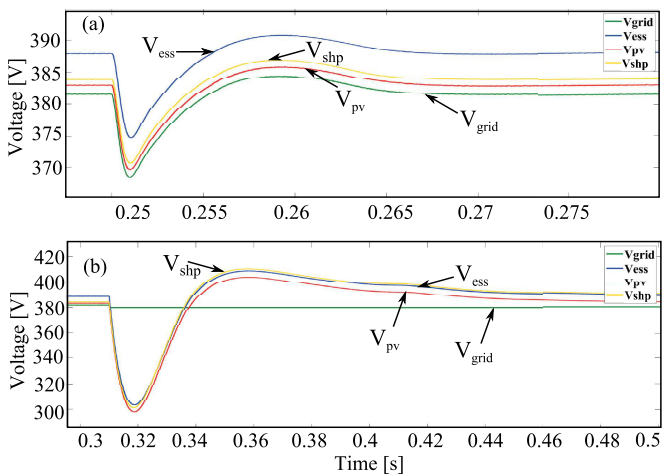


Fig. 9. (a) Load Connection response. (b) Grid Disconnection-Island operation mode

In Fig. 10 is compared the performance of the DC-link voltage against its references. Note that the signal follows the behaviour of the voltages in Fig. 8 and Fig. 9, but tracking the nominal voltage reference.

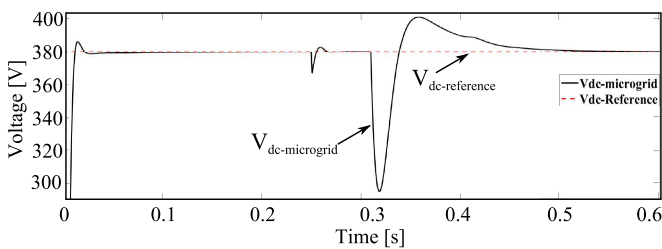


Fig. 10. DC-Link voltage behaviour

In Fig. 11 it is shown the performance of DG's converters internal current. The grid feeding nodes response is compared

with the respective reference value, is clear that these nodes exceed the current control performance. The case of the SHP source is not less important. A fast response against disturbances ensures the stability of the microgrid, even without utility grid support.

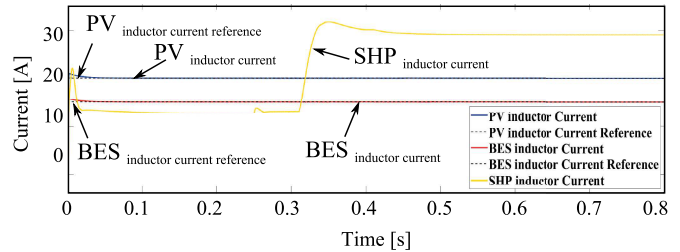


Fig. 11. Distributed generators inductor currents response

Other information about the controller's response is available in Fig. 12. The internal control signal's performance (duty cycle) shows smooth changes against the disturbances and no saturation even in the isolation process.

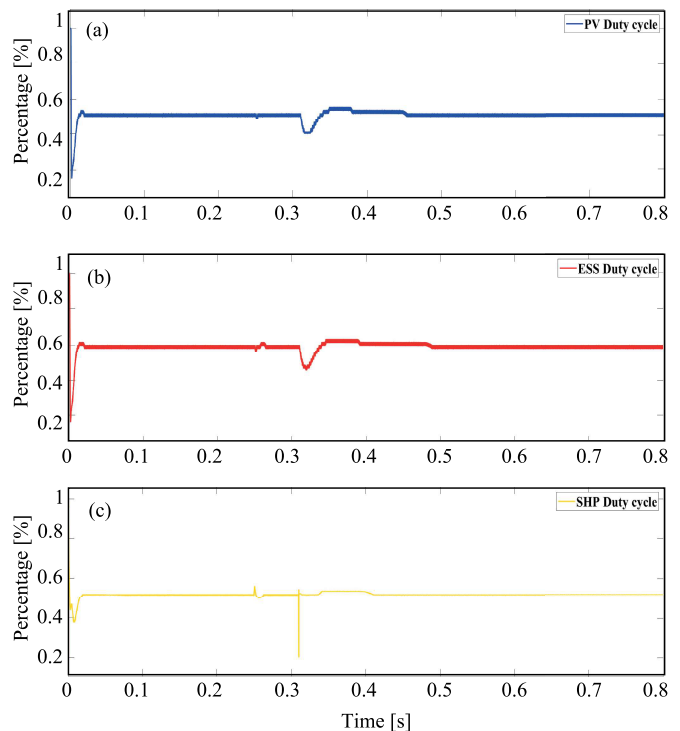


Fig. 12. Duty cycle of the distributed generators response: (a) Photo-Voltaic (PV) Node, (b) Battery Energy Storage (BES) node, (c) Small Hydro Power (SHP) node

In Fig. 13 is shown the duty cycle during the transient response.

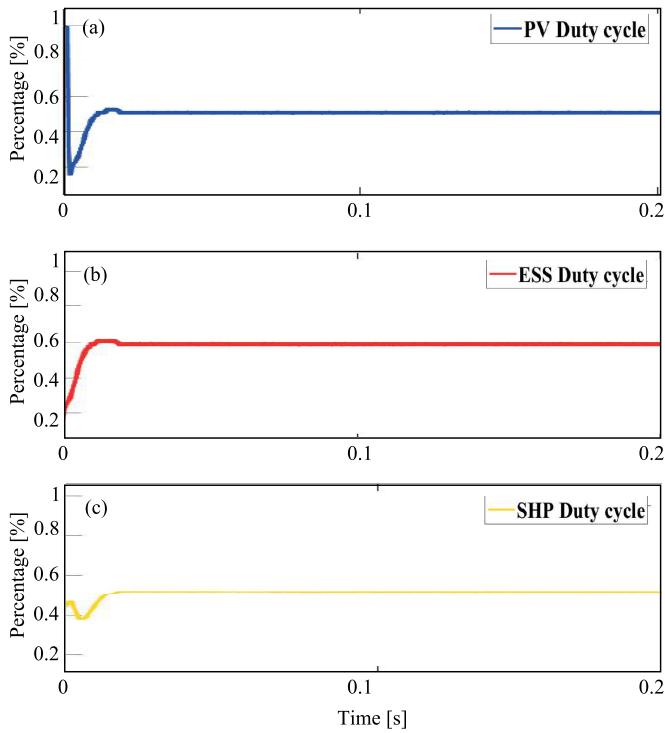


Fig. 13. Transient response of the duty cycle of the distributed generators response: (a) Photo-Voltaic (PV) Node, (b) Battery Energy Storage (BES) node, (c) Small Hydro Power (SHP) node

In Fig. 14 is shown the duty cycle during the disturbance.

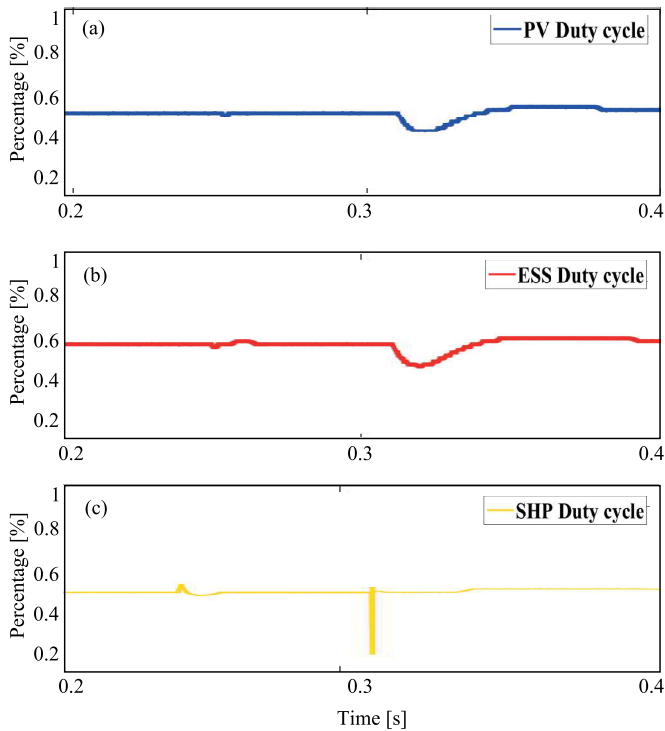


Fig. 14. Disturbance response of the duty cycle of the distributed generators response: (a) Photo-Voltaic (PV) Node, (b) Battery Energy Storage (BES) node, (c) Small Hydro Power (SHP) node

An interesting behavior is depicted in Fig. 15, which shows the current consumption at the load converters input. When this graph is compared with Fig. 6(a), is possible to check that the addition of all the DG's current injection is equal to the addition of all the load input current consumption. In

Fig. 10, it is important to note the disturbances effects among the graphs. The addition of extra load in  $L_1$  at  $t = 250ms$  causes a sudden current increase in the  $I_{L1}$ , but this doesn't affect the behavior of the rest of the load nodes drastically. Instead, the microgrid's disconnection at  $t = 310ms$  visibly affects  $L_3$ . Since this load is directly connected to the DC-link, the current is dependent on its variations.

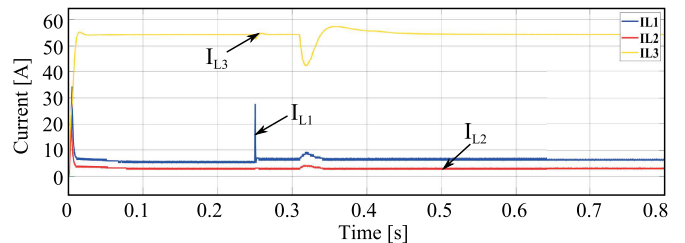


Fig. 15. Current consumption of the DC-DC interfaces and the Load 3.

Finally, in order to check the controller's sturdiness, Fig. 16(a) shows the response of the currents at the output of the DC-DC interfaces, is clear that the first disturbance increases the current consumption in a 20% of the original value; out of that, any disturbance is visible through all the simulation time. Fig. 16(b) shows the output voltage of the load DC/DC interfaces compared with the reference values. The first disturbance triggers a slight voltage loss that is quickly corrected.

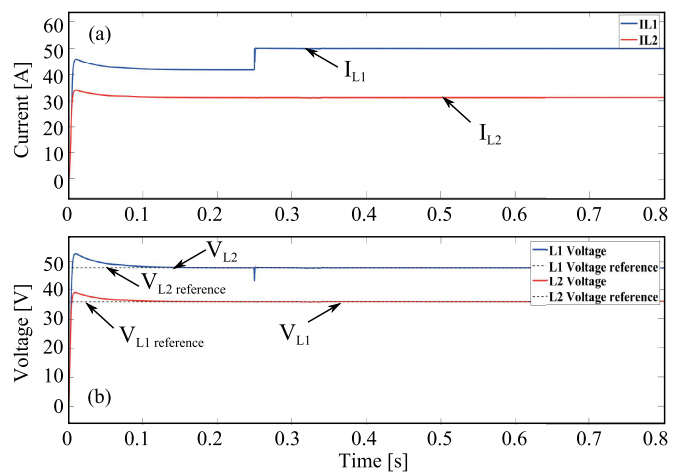


Fig. 16. (a) Loads Current consumption, (b) DC-DC interfaces output voltages

In Fig. 17 is depicted as the behavior of the load interfaces' duty cycle. The ability to read the input voltage changes improves the performance of the EFL inner controllers.

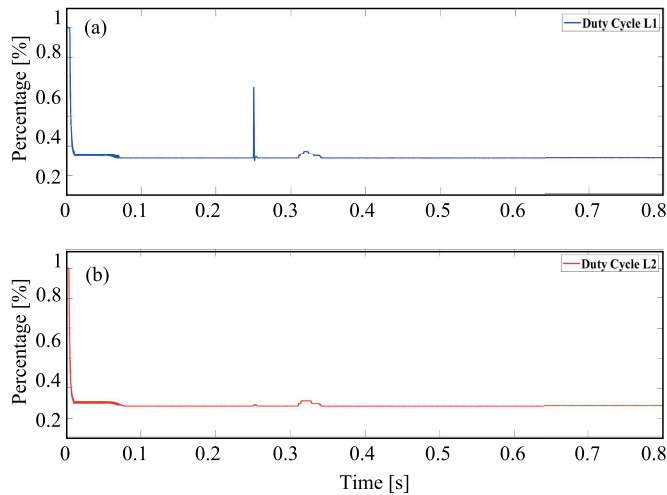


Fig. 17. Duty Cycle of the load DC-DC interfaces: (a) Load 1, (b) Load 2

#### IV. CONCLUSION

In this work, a novel hierarchical linear-nonlinear controller is proposed and validated over several scenarios that validated the controller's robustness, including two types of disturbances and island operation mode. The control signals and reference tracking signal for each node are discussed, where the proposed approach demonstrates its performance in each of the tested scenarios. In addition, it can be seen that the proposed approach successfully manages the inclusion of disturbances, three types of distributed generation units, and also island operation mode. As future works, comparison analysis of hierarchical structures that include linear-linear or linear-nonlinear structures is proposed over several types of DC microgrids. This analysis can be made in order to evaluate the adequate hierarchical controller features for a microgrid structure with distributed generation units.

#### REFERENCES

- [1] J. S. Velez-Ramirez, L. A. Rios-Norena, and E. Giraldo, "Buck converter current and voltage control by exact feedback linearization with integral action," *Engineering Letters*, vol. 29, no. 1, pp. 168–176, 2021.
- [2] F. Osorio-Arteaga, J. J. Marulanda-Durango, and E. Giraldo, "Robust multivariable adaptive control of time-varying systems," *IAENG International Journal of Computer Science*, vol. 47, no. 4, pp. 605–612, 2020.
- [3] J. S. Velez-Ramirez, M. Bueno-Lopez, and E. Giraldo, "Adaptive control approach of microgrids," *IAENG International Journal of Applied Mathematics*, vol. 50, no. 4, pp. 802–810, 2020.
- [4] B. Hernandez, E. Giraldo, S. Ospina, and A. Garces, "Master-slave operation of DC microgrids: An adaptive control approach with estimation," in *4th IEEE Colombian Conference on Automatic Control: Automatic Control as Key Support of Industrial Productivity, CCAC 2019 - Proceedings*, 2019.
- [5] B. R. Naidu, G. Panda, and B. C. Babu, *Dynamic energy management and control of a grid-interactive DC microgrid system*. Elsevier Inc., 2019. [Online]. Available: <http://dx.doi.org/10.1016/B978-0-12-812154-2.00003-1>
- [6] F. Gao, R. Kang, J. Cao, and T. Yang, "Primary and secondary control in DC microgrids: a review," *Journal of Modern Power Systems and Clean Energy*, vol. 7, no. 2, pp. 227–242, 2019. [Online]. Available: <https://doi.org/10.1007/s40565-018-0466-5>
- [7] M. A. Hassan, E. Li, X. Li, T. Li, C. Duan, and S. Chi, "Adaptive passivity-based control of dc-dc buck power converter with constant power load in dc microgrid systems," *IEEE Journal of Emerging and Selected Topics in Power Electronics*, vol. 7, no. 3, pp. 2029–2040, 2019.
- [8] X. Li, X. Zhang, W. Jiang, J. Wang, P. Wang, and X. Wu, "A novel assorted nonlinear stabilizer for dc-dc multilevel boost converter with constant power load in dc microgrid," *IEEE Transactions on Power Electronics*, vol. 35, no. 10, pp. 11 181–11 192, 2020.
- [9] F. Ni, L. Yan, J. Liu, M. Shi, J. Zhou, and X. Chen, "Fuzzy logic-based virtual capacitor adaptive control for multiple HESSs in a DC microgrid system," *International Journal of Electrical Power and Energy Systems*, vol. 107, no. May 2018, pp. 78–88, 2019. [Online]. Available: <https://doi.org/10.1016/j.ijepes.2018.11.023>
- [10] R. Heyderi, M. Alhasheem, T. Dragicevic, and F. Blaabjerg, "Model predictive control approach for distributed hierarchical control of vsc-based microgrids," in *2018 20th European Conference on Power Electronics and Applications (EPE'18 ECCE Europe)*, 2018, pp. P.1–P.8.
- [11] S. Peyghami, H. Mokhtari, and F. Blaabjerg, *Hierarchical Power Sharing Control in DC Microgrids*. Elsevier Inc., 2016. [Online]. Available: <http://dx.doi.org/10.1016/B978-0-08-101753-1.00003-6>